Available online at www.sciencedirect.com
ScienceDirect
Energy Reports 8 (2022) 1092–1106
www.elsevier.com/locate/egyr

TMREES22-Fr, EURACA, 09 to 11 May 2022, Metz-Grand Est, France

# Performance analysis of a large TES system connected to a district heating network in Northern Italy

Mariagrazia Pilotelli[a,*], Benedetta Grassi[a], Daniele Pasinelli[b], Adriano M. Lezzi[a]

[a] *Department of Mechanical and Industrial Engineering, University of Brescia, 25123 Brescia, Italy*
[b] *A2A Calore & Servizi S.r.l., 25124 Brescia, Italy*

Received 19 June 2022; accepted 19 July 2022
Available online xxxx

**Abstract**

The addition of storage capacity to district heating systems increases flexibility and expands the range of usable heat sources. Despite their apparently simple nature, thermal energy storage (TES) tanks display a wide range of performances due to different construction and operation choices, as proven by numerous literature studies. However, most of the investigations focus on domestic-size tanks of few cubic metres or, on the other hand, very large seasonal storages of hundreds of thousands of cubic metres. In this work, the performances of a 5000 $m^3$ TES recently introduced in a district heating network in Brescia, Italy, are experimentally analysed using temperature and flow rate measurements acquired over two months in the heating season. First-law efficiencies, exergy, and stratification parameters are calculated and discussed. Energy and exergy efficiencies computed for all examined cycles are above 90%, in line with literature values for smaller and larger TESs. The thermocline profile is generally stable through the cycle unless anomalous events occur, and its average thickness is below 4% of the water height. The combined analysis of single-point indicators, thermocline profiles, and qualitative temperature heatmaps shows that short partial charge/discharge events followed by long stand-by periods negatively affect performances. Stratification efficiency and stratification number give further time-dependent information on the vertical distribution of temperatures in the TES. Heat losses towards the outside are also estimated and discussed in the light of integrative measurements performed on other TESs with similar characteristics, showing that particular care must be paid to the top, where dissipation could be increased by evaporation phenomena if the water surface is not protected.


Peer-review under responsibility of the scientific committee of the TMREES22-Fr, EURACA, 2022.

*Keywords:* Thermal energy storage; District heating; Thermal stratification; Thermocline; Exergy; Efficiency

* Corresponding author.
*E-mail address:* mariagrazia.pilotelli@unibs.it (M. Pilotelli).

https://doi.org/10.1016/j.egyr.2022.07.094


Peer-review under responsibility of the scientific committee of the TMREES22-Fr, EURACA, 2022.

**Nomenclature**

| | |
|---|---|
| $c_p$ | Specific heat of water |
| $D$ | Diameter |
| $Ex$ | Exergy |
| $H$ | Height |
| $m$ | Mass of water |
| $M$ | Moment of energy |
| $MIX$ | Mixing number |
| $Str$ | Stratification number |
| $t$ | Time |
| $T$ | Thermodynamic temperature |
| $z$ | Height |

**Greek letters**

| | |
|---|---|
| $\eta$ | Efficiency |
| $\rho$ | Density |
| $\upsilon$ | Volumetric flow rate |
| $\psi$ | Exergy efficiency |

**Subscripts**

| | |
|---|---|
| ch | Charge |
| dis | Discharge |
| exp | Experimental |
| h | High |
| in | Inlet |
| l | Low |
| max | Maximum |
| min | Minimum |
| mix | Fully mixed |
| out | Outlet |
| str | Stratification |
| strat | Perfectly stratified |

**Abbreviations**

| | |
|---|---|
| TES | Thermal energy storage |
| DH | District heating |

## 1. Introduction

District heating (DH) systems are evolving to incorporate different energy sources and provide more efficient operation. The introduction of thermal energy storage (TES) elements is the traditional method to make the network flexible enough to manage the time gap between demand and supply [1], and the distance gap between generation and consumption [2]. This is especially true in the case of expansion of existing networks with renewable energy, waste heat sources, or heat pumps [3], as storage systems are known to help both in handling production surpluses and in covering load peaks [4].

Despite their apparent simplicity, TESs can have very different performances depending on construction and operation choices, as outlined by literature studies and confirmed by experimental evidence. For example, Saloux and Candanedo [5] explore the influence of storage sizing and energy injection/extraction rate on primary energy

saving by simulation. Lou et al. [6] review the influence of design and operation parameters, such as flow rate, working temperature, flow distribution, and inlet/outlet position, on the thermocline performances, while [7] analyse the technical aspects and economic feasibility of four types of seasonal TES systems, showing a considerable impact of storage shape on energy, exergy and stratification performances.

The characterisation of TES systems to be included, or already installed, in a DH network is therefore of interest for the utility company A2A Calore & Servizi on three levels:

- To improve the design of storage tank systems to increase the usable energy
- To enable more accurate predictions on the usable energy for management purposes
- To identify operation practices to fulfil the demand without compromising the quality of the stored energy
- To optimise the TES maintenance activities by improving the safety level while lowering the operational expenditure.

Performance indicators are a possible way to characterise TES and compare different options with each other. Most common evaluations concern first-law energy efficiencies, exergy, stratification, and hydrodynamic behaviour [6]. As pointed out by Haller et al. [8], not all the indicators can be equally used during all cycle stages, and different indicators give different information; for example, some of them only provide overall quantities relative to the specific cycle under investigation (such as useful energy that can be discharged, or degree of mixing), while other ones are built to give time-dependent information (such as the period in which most of the destratification occurs). For this reason, several indicators are usually computed based on simulations or experimental measurements to evaluate the TES performances from different perspectives. Examples of similar analyses can be found in the works by Castell et al. [9] Dahash et al. [7], Rendall et al. [10].

This approach can, in principle, be used for TESs of any size, but, in general, the results obtained for a specific storage tank cannot be extended to other systems, especially if they have very different capacities, constructive features, and operating cycles. Most of the studies in the literature concern small tanks, suitable for residential applications and often coupled with thermal solar collectors. Such systems are experimentally easier to characterise than large TESs and are also of interest from an energy performance of buildings perspective [11]. Fernández-Seara et al. [12] experimentally test a 150 l storage cylinder for domestic hot water during dynamic operation to find the configuration of the inlet/outlet port that maximise energy, exergy, and stratification efficiencies. Siuta-Olcha and Cholewa [13] also consider a domestic hot water tank with 350 l capacity coupled with a thermal solar collector, focusing on stratification number and thermocline thickness over one summer month in Poland. A similar system is investigated numerically by [14], who calculate the transient temperature distribution in the axial direction and stratification-related indicators with different heat source combinations. On the other endpoint of the scale range, interest is recently growing towards very large water systems to be used as seasonal TESs, like in the simulation work by Dahash et al. [7]. Bai et al. [15] investigate numerically and experimentally the behaviour of a 3000 $m^3$ underground water pit with a focus on stratification behaviour over nine months. As a note, the study also shows that the amount of equipment and the complexity of the experimental set-up grow with storage size: the larger the system, the stronger the need to envisage measurement instruments already at the design stage. These are the main reasons why few experimental studies are available in the literature on TES systems of thousands of cubic metres.

To summarise, the need for experimental analyses on large storage systems is motivated by the variability in their performances and the limited availability of field studies in the current literature. This work focuses on the analysis of data collected on a 5000 $m^3$ storage tank installed in the DH network in Brescia, Italy, by utility company A2A. The TES, finished and put in operation in January 2020, features an injection and flow straightening device designed to minimise flow maldistribution and ensure good stratification performances [16]. To validate the effectiveness of the design, A2A Calore & Servizi included in the project of that TES thorough measurement equipment including temperature sensors, flow metres, and pressure gauges, extending this approach also to the projects of several other TESs built thereafter in the cities of Brescia, Bergamo, and Milano. These ‘living laboratories’ are precious sources of high-quality data over long periods and in regular operation. The performances are evaluated using energy, exergy, and stratification parameters, calculated over two winter months, and whose values are compared to literature studies. Transient charge/standby/discharge periods are also analysed, based on which recommendations are drawn about practices that could improve or, inversely, be detrimental to performances.

The TES, the experimental set-up, and the performance indicators used to characterise the system are described in Section 2. Results are shown and discussed in Section 3, whereas Section 4 summarises the main findings of the study and provides construction and operative recommendations. Conclusions are drawn in Section 5.

## 2. Materials and methods

### 2.1. TES characteristics and experimental set-up

The experimental analysis has been performed on a TES installed in the 'Lamarmora' power plant in the DH network of Brescia, Italy, managed by the local utility company A2A Calore & Servizi. The tank is a cylinder of diameter $D$ = 20 m and height $H$ = 20 m, with a permitted water level between 17.5 and 18.5 m (Fig. 1) and a top water surface at atmospheric pressure. The main structure is made of carbon steel with thickness varying from 8 mm at the bottom to 5 mm at the top, while thermal insulation is achieved with a 200 mm layer of mineral wool (Table 1). The tank features innovative upper and lower inlet and flow-straightening devices to promote stratification [16]. The system, co-designed by A2A and the University of Brescia, features a toroidal perforated manifold with high-velocity radial injection from the tank wall inwards, and a perforated plate. It is worth noting that in standard diffusers adopted in similar applications water usually enters the tank from a central point and flows outwards at low velocity. During operation, temperatures along the height of the TES are continuously measured by Pt100 temperature sensors installed in thermo-wells at different heights (10 equally spaced-apart sensors between 1.8 m and 15.3 m, plus two pairs at 0.75/0.95 m and 16.5/16.7 m right upstream and downstream of the flow straightening systems). The thermo-well tips – thus the Pt100 RTD sensors – are submerged in the hot water at a distance of 600 mm from the tank wall. Inlet and outlet flow rates are also measured. Details about the measurement equipment are given in Table 2. The analysis in this paper is based on measurements collected over two months (December 2020–January 2021) and provided as a weighted average on 300 s. Nominal minimum and maximum water temperatures are 60 °C and 97 °C, respectively. Considering water density and specific heat at the average temperature of 78 °C, the theoretical capacity of the TES is 202 MWh. During the measurement period, the heat stored by the TES with respect to the nominal minimum temperature has been above 180 MWh for less than 15% of the time (Fig. 2). Preliminary measurements from a more recent system built in the same DH network and consisting of two 2200 $m^3$ tanks are also presented limitedly to heat losses analysis. Such tanks, located in the 'Centrale Nord' power plant in the same DH network, feature a similar inlet diffuser as the 'Lamarmora' TES.

**Table 1**. Mechanical and thermal properties of TES materials.

| Element | Description | Property [unit] | | | |
|---|---|---|---|---|---|
| | | Thermal conductivity [W/(m K)] | Density [kg/$m^3$] | Thickness [mm] | Young's modulus [MPa] |
| Cylinder structure | Slit strip of structural steel | 42 | 7800 | 5…8 | 470…630 |
| | | Thermal conductivity [W/(m K)] | Density [kg/$m^3$] | Thickness [mm] | Specific heat [J/(kg K)] |
| Lateral surface insulation | Rigid mineral wool | 0.045 | 100 | 20 | 840 |
| Top insulation | Rigid mineral wool | 0.039 | 155 | 20 | 1030 |

Data have been made available by the utility company A2A Calore & Servizi as spreadsheet files and post-processed with Python scripts. The study focuses on evaluating the TES performances in terms of usable energy. Therefore, it considers heat losses towards the external environment, amount of mixing, and stratification quality. In particular, temperature and flow rate experimental data are used to:

- calculate the values of energy-, exergy- and stratification-related indicators, and evaluate them with respect to other TES systems for which similar studies are found in the literature;
- qualitatively examine the impact of operative practices on the performances and provide recommendations to minimise negative effects and improve efficiency.

Definitions and calculation details for the performance indicators are described in the following subsections.

### 2.2. Performance indicators

Several indicators to characterise TES systems are reported in the literature. According to [6], three categories can be identified to determine first- and second-law efficiency (category 1), stratification-related indicators (category 2),

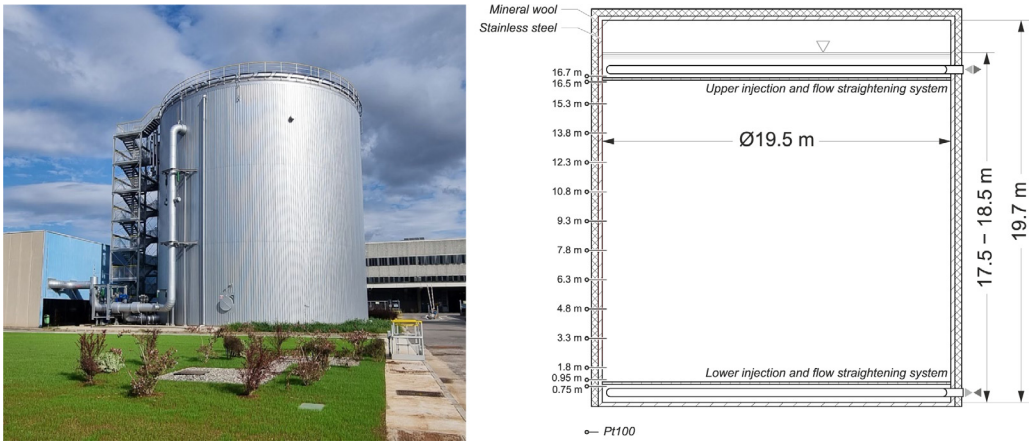


**Fig. 1.** Storage tank installed in 'Lamarmora' power plant, Brescia DH network. Construction timelapse video available online [17].

**Table 2**. Characteristics of the measurement instruments installed on the analysed TES (m.v.: measured value).

| Quantity | Sensor type | Range | Maximum error |
|---|---|---|---|
| Temperature | Pt100, 3 wire | 0…150 °C | ±(0.278% m.v. + 0.20 K) |
| Flow rate | Ultrasonic | 0…2000 $m^3$/h | ±(0.3% m.v. + 2 mm/s) |

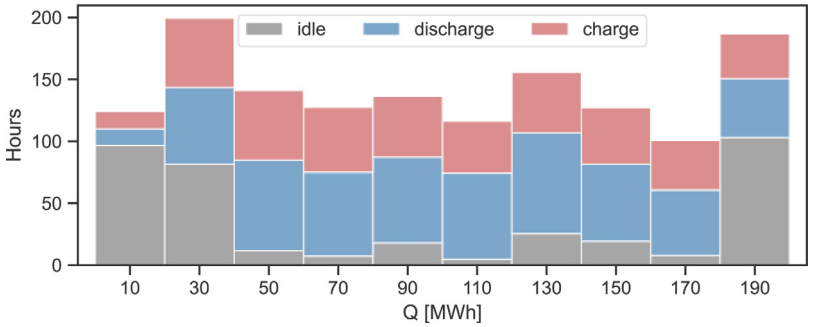


**Fig. 2.** Breakdown of stored heat with respect to minimum nominal temperature in the measurement period (bin width: 20 MWh). .

and thermal and hydrodynamic characteristics (category 3). In this work, category 1 and category 2 parameters are calculated, since they allow to identify the processes that can lead to a reduction of usable energy with respect to theoretical potentiality.

First-law efficiencies quantify fractions of energy with respect to total capacity, the choice of reference temperatures depending on the objective of the estimation. In this work, definitions by Zurigat and Ghajar [18] of discharging and charging efficiencies are used. Charging (or storage) efficiency $\eta_{ch}$ is calculated as

$$\eta_{ch} = \frac{\int_0^{t_{ch}} \rho \upsilon(t) c_p \left(T_{in} - T_{out}\left(t\right)\right) dt}{m_{TES} c_p \left(T_{in} - T_{1}\right)} \tag{1}$$

Here, $T_{out}(t)$ is the time-dependent extraction temperature (that is, the temperature measured by the lowermost temperature sensor), $\rho\upsilon(t)$ is the time-dependent mass flow rate, $m_{TES}$ is the mass of water in the TES, and $T_{in}$ is the inlet temperature, taken as the maximum temperature value over the cycle since it does not vary significantly during the process. $T_1$ represents the initial temperature of the cold water in the TES, thus it is calculated as the average temperature at the initial time step. The integral is made between the initial time and the time $t_{ch}$ at which the extraction temperature exceeds a certain threshold, indicating the presence of a layer at intermediate temperature (thermocline). The usable charged energy is then related to the total energy that could be stored in the

TES, calculated as the product of water thermal capacity $m_{TES}\ c_p$ and temperature difference between inlet hot water and initially cold storage. Indeed, in a perfectly stratified storage with a sharp interface between hot and cold fluid, $t_{ch}$ would be achieved when the tank is filled with water at the maximum temperature, and $\eta_{ch}$ would be equal to 1. In a real storage tank, the thicker the thermocline, the shorter the time $t_{ch}$, and the lower the numerator in Eq. (1). The charging efficiency, therefore, represents a measure of the usable energy that is stored in the TES during the charging process.

Discharging efficiency $\eta_{dis}$ is defined analogously as the ratio between the useful heat delivered during the discharge process and the stored heat at the initial time step of the process:

$$\eta_{dis} = \frac{\int_0^{t_{dis}} \rho \upsilon(t) c_p \left(T_{out}(t) - T_{in}\right) dt}{m_{TES} c_p \left(T_h - T_{in}\right)} \tag{2}$$

where $T_{out}(t)$ is the time-dependent extraction temperature (that is, the temperature measured by the uppermost temperature sensor). $T_{in}$ is the temperature of the water returning from the users, whose value is calculated as the average of the cold-water temperature in the TES at the end of the discharge. The sum at the numerator is "stopped" at time $t_{dis}$, when the extraction temperature falls below a usability threshold defined according to the specific needs. The reference energy at the denominator is calculated based on the temperature difference between the cold inlet water $T_{in}$ and the initial temperature at the beginning of the discharge process, $T_h$. The latter value is rarely uniform in practice; therefore, it was chosen to calculate it as the temperature of a storage with equivalent usable energy (where 'usable' is defined with the same criterion adopted to calculate $t_{dis}$) as the one contained in the TES at the beginning of the discharge process. In this way, the discharging efficiency represents the portion of usable energy that is extracted during the process.

As a possible criterion to define the usability thresholds, Zurigat and Ghajar [18] propose that the outlet-to-inlet temperature difference does not fall below 20% of the initial value. In this work, similar criteria are used, but fixing the endpoints as the maximum and minimum design values for the given TES. The usability thresholds during charge and discharge processes are, respectively:

$$\left(T_{out,max}\right)_{ch} = T_{out}\left(t_{ch}\right) = T_{min} + 0.2\ \left(T_{max} - T_{min}\right) \tag{3a}$$

$$\left(T_{out,min}\right)_{dis} = T_{out}\left(t_{dis}\right) = T_{min} + 0.8\ \left(T_{max} - T_{min}\right) \tag{3b}$$

In the case at hand, temperature endpoints are $T_{max} = 370$ K and $T_{min} = 333$ K, thus the limit temperatures for charge and discharge processes are around 340 K and 363 K (67 and 90 °C), respectively.

The experimental application of Eqs. (1)–(2) with the previously described choices does result in $\eta_{ch}$ and $\eta_{dis}$ values calculated based on different energy storage potentialities, mainly due to storage temperature evolutions during idle and stand-by periods. This aspect must be considered when comparing the calculated values to each other.

For a complete charge/discharge cycle, the first-law energy efficiency $\eta_I$ can be computed by dividing the discharged usable energy (the numerator in Eq. (2)) by the usable energy stored at the end of the charging process (the numerator in Eq. (1)). This parameter gives an estimation of the portion of energy that becomes unusable during stand-by and discharge periods. Another useful indicator in this respect is the exergy efficiency $\psi$, which takes into consideration the generation of entropy during the cycle, and is defined as:

$$\psi = \frac{Ex_{dis}}{Ex_{ch}} \tag{4}$$

Here, $Ex_{ch/dis} = \rho\ \upsilon_{ch/dis}\ c_p\ [(T_{ch,in/dis,out} - T_{ch,out/dis,in}) - T_0 \ln\left(T_{ch,in/dis,out}/T_{ch,out/dis,in}\right)]$. $T_{ch,in}$ and $T_{dis,in}$ are water inlet temperatures during charge and discharge processes, respectively, while $T_{ch,out}$ and $T_{dis,out}$ are the corresponding extraction temperatures. $T_0$ is the average ambient temperature during the considered period, estimated as 277.5 K based on public weather station data. Considering a complete charge/discharge cycle as the reference period, $\psi$ is related to the fraction of the initially charged exergy that is destroyed during the following stand-by and discharge phases; therefore, a correlation is expected with previously defined energy efficiency $\eta_I$.

To gain more information about stratification and mixing processes, two time-dependent parameters are also calculated. Stratification efficiency $\eta_{str}$ is a measure of the stratification degree of the TES in a stratification scale ranging from fully mixed to perfectly stratified storage, the two ideal endpoints having the same energy content as

the experimental TES [19]. The stratification efficiency is related to mixing number *MIX* originally introduced by [20], and it can be written as

$$\eta_{str}(t) = 1 - MIX(t) = \frac{M_{exp}(t) - M_{mix}(t)}{M_{strat}(t) - M_{mix}(t)} \tag{5}$$

where symbol $M$ indicates a moment of energy, defined similarly to the first moment of inertia. The moment of energy of the experimental layer is given by $M_{\text{exp}} = \Sigma_{(j=1\ldots J)}\ [z_j \cdot \rho\ \text{c}_p\ V_j \cdot T_j]$, with $J$ number of layers for which a temperature measurement is available, $z_j$ elevation of the layer (measurement point) and $V_j$ and $T_j$ volume and absolute temperature of the $j$th layer, respectively. In this work, the moments of energy of the theoretical storages are calculated so that they have the same energy content as the actual TES at any time, as in [21]. In particular, the moment of energy of the perfectly stratified TES is calculated using the lowest and highest temperatures recorded during the whole measurement period. Stratification efficiency highlights time-dependent information, such as destratification events for example due to heat losses, heat transfer between hot and cold fluid, or mixing.

Complementary information can be obtained by the stratification number $Str(t)$, defined by Fernández-Seara et al. [12] as the ratio between the mean temperature gradient in the TES for a given process (charge/discharge) and the maximum mean temperature gradient during that process. Defining $\Delta z_j$ the height of the $j$th layer, and $T_{\text{max,cy}}$ and $T_{\text{min,cy}}$ the maximum and minimum temperatures recorded in the cycle, stratification number is calculated as

$$Str\ (t) = \frac{\overline{\left(\frac{\partial T}{\partial z}\right)_t}}{\left(\frac{\partial T}{\partial z}\right)_{\max}} = \frac{\frac{\sum_{j=1}^{J-1}(T_{j+1}-T_j)}{\sum_{j=1}^{J-1}\Delta z_j}}{\frac{(T_{\max,\text{cy}}-T_{\min,\text{cy}})}{\sum_{j=1}^{J-1}\Delta z_j}} = \frac{\sum_{j=1}^{J-1}\left(T_{j+1}-T_j\right)}{T_{\max,\text{cy}}-T_{\min,\text{cy}}} \tag{6}$$

The stratification number averages gradients on the TES volume, thus it is suitable to describe phenomena in which the temperature endpoints become closer (for example, mixing). However, it cannot describe the stratification quality in terms of thermocline thickness: all the rest being equal, whether the same average gradient derives from a small gradient over the whole TES or from a large gradient between two adjacent layers, *Str* will be the same.

In Section 3, quantitative results are presented and compared to literature values. Due to the limited number of experimental works on tanks of similar size, most of the parameters are compared to the predictions by Dahash et al. [7] for a 100000 m$^3$ tank with $H/D = 1$, to the literature values in [2] for short-term thermal storage tanks for DH systems, and to several experimental works on domestic size applications.

### 2.3. Other parameters

In addition to efficiency and stratification-related indicators, other parameters are taken into consideration to characterise the performances of the TES.

Thermal energy losses towards the outside are evaluated by calculating the difference in the stored heat between the end of a full charge period and the moment before the beginning of the subsequent discharge period. This aspect is also examined by comparing the temperature profiles in two twin tanks operating in parallel, which differ only for the presence in one of them of a protective membrane above the water free surface.

As concerns stratification-related parameters, thermocline thickness is calculated separately for each charge and discharge process. The readings from temperature sensor $j$ during the process can be plotted against the time-dependent water mass displacement, calculated as $\Delta x_j(t) = \Delta x_{\text{period}} - \{\Sigma_{(\tau=0\ldots t)}\ [\delta\tau \cdot 4\upsilon(\tau)/(\pi \text{D}^2)] + (h_j - h_{\text{ref}})\}$. Here, $\Delta x_{\text{period}}$ is the total estimated displacement of the water mass at the end of a given charge or discharge period, $\delta\tau$ is the time step between two consecutive recordings, $\upsilon(\tau)$ is the measured volumetric flow rate, $h_j$ is the elevation of the $j$th sensor, and $h_{\text{ref}}$ is a reference position (in this case, the elevations of the charge/discharge inlet distribution systems). This strategy allows collapsing of the temperature curves obtained by all the temperature sensors to evaluate the stability of the thermocline in time. If the temperature profile is sufficiently stable, an average curve can be calculated, based on which an average thermocline thickness during the process is computed considering lower and upper thresholds determined through Eqs. (3a)–(3b).

Qualitative representations of the temperature evolution during each cycle are also drawn in the form of heatmaps as an immediate visualisation tool to assist the analyst in the interpretation of numeric results.

## 3. Results

### 3.1. Efficiency indicators

First-law charging efficiencies are calculated according to Eq. (1) on cycles featuring a charging process from completely cold to completely hot TES, this condition being evaluated based on the threshold in Eq. (3a). A similar calculation has been done of discharging efficiencies according to Eq. (2) for cycles featuring a complete discharge process and with usability condition defined according to Eq. (3b). All calculated efficiency values as a function of average flow rate and their distributions are shown in Fig. 3. Charging efficiencies are between 95% and 96%, whereas discharging efficiencies fall in the range of 91%–94%. Despite the considerable difference in size and application, these values are in line with findings by Fernández-Seara et al. [12], who report maximum discharging efficiencies of 95% and maximum charging efficiencies above 90%. Similar figures can also be found in [2] and in [7] for large-size storage tanks. It is believed that the lower values of $\eta_{dis}$ with respect to $\eta_{ch}$ are mainly due to the different cold-water temperatures during the two processes: at the initial time of a charging period, cold water is generally warmer than it is at the end of the next discharging period, thus $\eta_{ch}$ is calculated with smaller denominator than $\eta_{dis}$. A slight dependency of discharging efficiencies on how quickly the process occurs is found: the lower the fluid speed, the higher the fraction of heat that is made unusable during the draw-off. However, in-between stand-by periods seem to have an even larger influence. As an example, the scatter plot on the left of Fig. 3 shows a relatively low discharging efficiency for cycle ID 22. In Fig. 4, the heatmap representing the vertical temperature evolution in the TES during this cycle highlights the presence of a short discharge period (h. 12:30 20/12) which creates a layer of cold water below the flow distributor and promotes the transfer of heat from hot to cold water. Moreover, the actual discharge process starts almost one day later. In the case of cycle 22, it can be concluded that the combination of introducing a small amount of cold water on the bottom and leaving the system in stand-by for a long time reduced the amount of usable heat with respect to the initial stored energy.

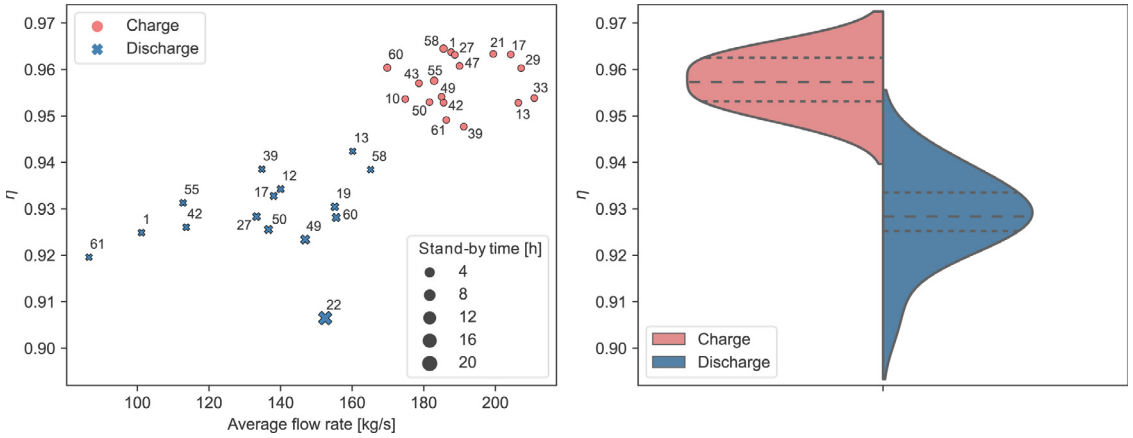


**Fig. 3.** Charging/discharging efficiencies, labelled with cycle identifiers, as a function of average flow rate (left). Charging/discharging efficiency distributions, with mean, first and third quartile indicated as dashed lines (right).

In the case of cycles featuring a complete charge followed by a complete discharge ('full cycles'), it is possible to connect the performances of the TES in the two phases by employing discharge-to-charge first-law efficiency $\eta_I$ and exergy efficiency $\psi$. Fig. 5 shows the correlations between energy and exergy parameters: on the left scatter plot, only a weak correlation emerges between charging and discharging efficiencies, and no definite relation can be found between these two indicators and exergy efficiency (represented by the colour and size of the markers). A stronger correlation is found between exergy efficiency and the discharge-to-charge efficiency, calculated as the ratio between the numerators $\eta_{dis}$ of and $\eta_{ch}$: this evidence suggests that both $\psi$ and $\eta_I$ are good indicators of the amount of stored usable energy that is lost during stand-by and discharge processes. In terms of values, exergy efficiencies lie between 92% and 99%, which demonstrates the excellent performance of the TES and is on average 10% higher than simulated by Dahash et al. [7] in the case of very large tanks with similar insulation thickness. These figures are far from the 20% limit reported by Guelpa and Verda [2] for seasonal systems, which can be penalised by very long stand-by and idle periods.

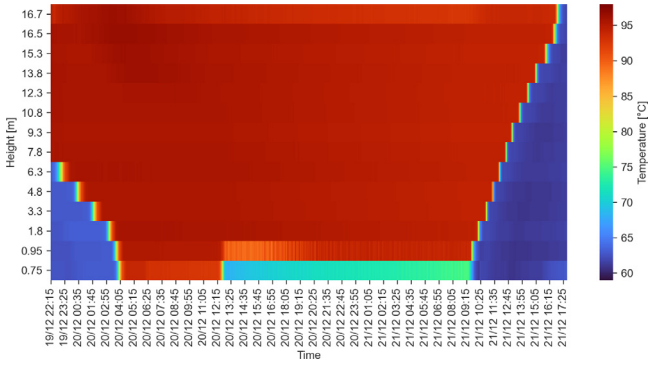


**Fig. 4.** Qualitative illustration of water temperature evolution in the TES during cycle 22 (axes not in scale).

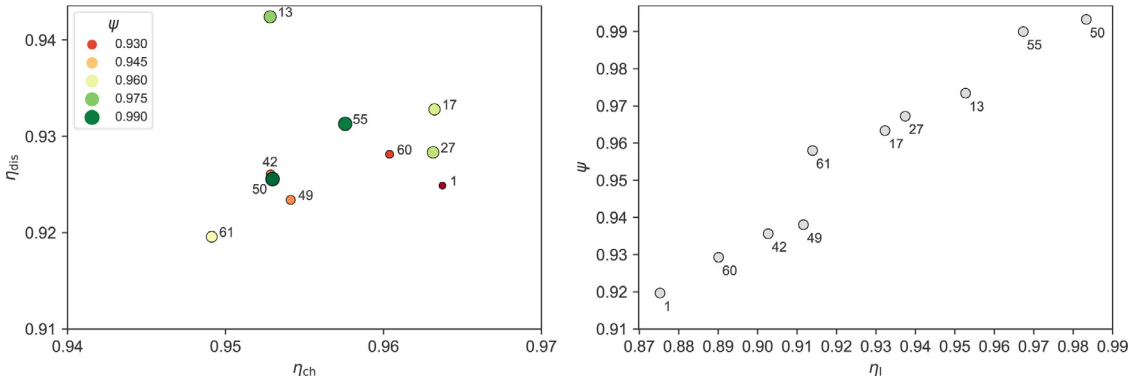


**Fig. 5.** Left: discharging efficiency vs. charging efficiencies for full cycles; colour and size of the markers represent exergy efficiencies. Right: exergy efficiencies as a function of discharge-to-charge efficiencies.

### *3.2. Thermal losses towards the outside*

Another potential source of energy waste is the loss of heat through the walls of the storage tank. To make an estimation, over 20 stand-by periods after charge processes have been isolated, and the difference between initial and final stored energy has been computed for each of them. It was found that 0.005% to 0.28% of stored heat was lost towards the outer environment along periods ranging from 25 min to 6 h. Neglecting the thermal storage capacity of the TES walls, a steady-state approximation based on an equivalent thermal circuit, with TES characteristics presented in Section 2.1, largely underestimates thermal losses. The source of this discrepancy is arguably due to the underestimation of the losses through the top area. Water does not fill the tank completely, as the maximum permitted level is more than one metre below the upper cover (see Fig. 1), where open ports for air venting are also present and act as thermal bridges towards the outside. To avoid the direct contact of the water surface with the atmosphere and the consequent oxygen absorption, a protective membrane can be laid and anchored to the tank wall. Such a layer also prevents evaporated water from escaping through the vents.

The membrane effect on thermal loss reduction has been observed in preliminary readouts from two identical 2200 $m^3$ TESs recently installed in the ‘Centrale Nord’ power plant of the Brescia DH network, featuring the same inlet diffusers as the TES in ‘Lamarmora’. The two tanks, shown in left Fig. 6, have $D = H = 15$ m and are connected in parallel, with an upper protective membrane installed in only one of them (‘East’). The inside of the ‘East’ tank is depicted in right Fig. 6, where the membrane anchored to the walls and the outlet vents on the top are visible. The comparison of time-dependent temperatures provided in Fig. 7 for three measurement points suggests that higher temperature values are reached in the TES featuring the protection, indicating that the membrane effectively helps in reducing heat losses from the upper surface due to convection and evaporation. The daily amount of evaporated

**Fig. 6.** Left: TESs in 'Centrale Nord', Brescia, Italy. Construction timelapse video available online [22]. Right: protective membrane installed in 'East' TES.

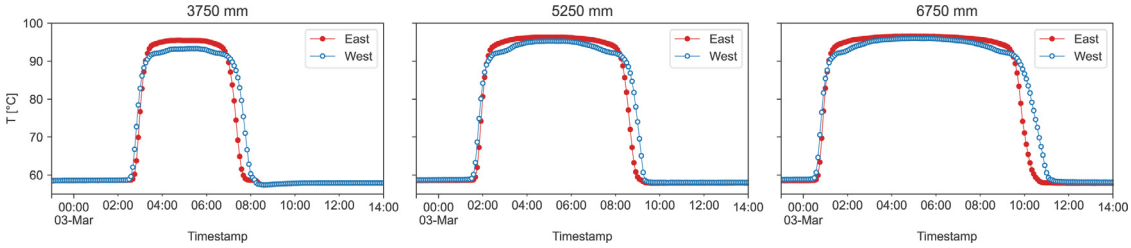


**Fig. 7.** Temperatures measured at different heights of 'Centrale Nord' twin TESs, with ('East') and without ('West') protective membrane.

water from the 'West' TES was experimentally estimated as 2 $m^3$, corresponding to a latent heat loss of around 1.2 MWh/d.

### *3.3. Stratification analysis*

Stratification quality has been initially investigated by calculating thermocline thicknesses for all cycles (that is, cycles featuring either partial or complete charge and discharge periods). The shape of the temperature profiles obtained from the experimental measurements generally remains quite stable over time, thus it is reasonable to calculate the thermocline thickness on the average curve, as explained in Section 2.3. On average, the thermocline thickness is 0.62 m (∼3.5% of the water height) with slightly larger variability for charge periods (Fig. 8). This order of magnitude is comparable with experimental evidence for smaller size TESs, like for example in [13], or even for chilled water tanks [23]. It is worth remarking that the same cut-off temperatures should be used when comparing thicknesses from different sources: for instance, to make a comparison with literature data in which 10% is used instead of 20% to define temperature thresholds according to Eqs. (3a)–(3b), thicknesses in Fig. 8 should be multiplied approximately by 2.5.

The outlier of 4th January 2021 (cycle ID 38) has been examined in detail. From the qualitative inspection of the hours preceding the charge (Fig. 9a), it is found that a plug of water at intermediate temperature is created on the top, possibly as a result of a short charge operation followed by a stand-by period, in which the small quantity of hot water introduced had the time to mix with cold water in the region above the flow distributor. When the actual night charge period starts, this layer is moved downwards and is not expelled until the end of the subsequent discharge period. Consequently, the thermocline thickness remains anomalously high throughout the whole cycle. Figs. 9b and 9c allow to compare cycle 38 with cycle 39, where a thinner thermocline thickness appears to be restored after the complete discharge of the TES. The estimated unusable heat associated to the thermocline in cycle 38 is almost 9% of the maximum storage capacity of the TES, against 3.3% of cycle 39. Figs. 9b and 9c also confirm that temperature profiles obtained from sensors at different elevations overlap, making the estimation of the thickness on the average curve a reasonable approximation for the entire process.

Stratification and destratification events have been also examined by calculating the time-dependent stratification efficiency $\eta_{str}(t)$ and stratification number Str($t$) for the twelve full cycles isolated in the measurement period, according to the definitions in Section 2.2.

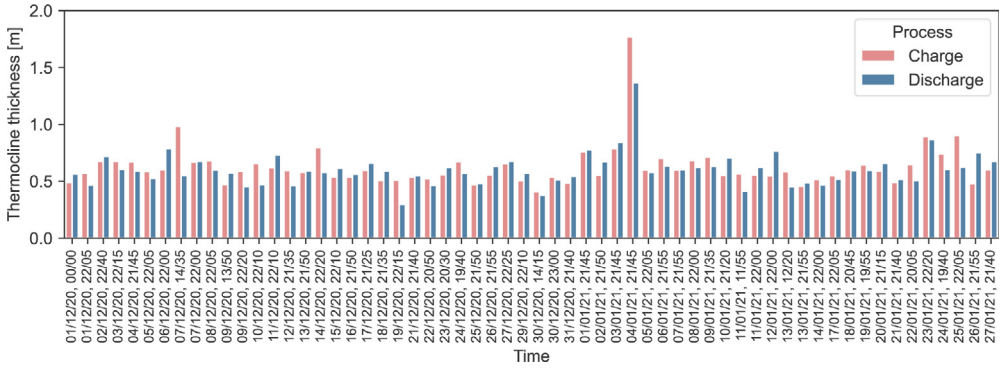


**Fig. 8.** Thermocline thicknesses in charge and discharge periods (cut-off dimensionless temperatures 0.2–0.8, abscissa not in scale).

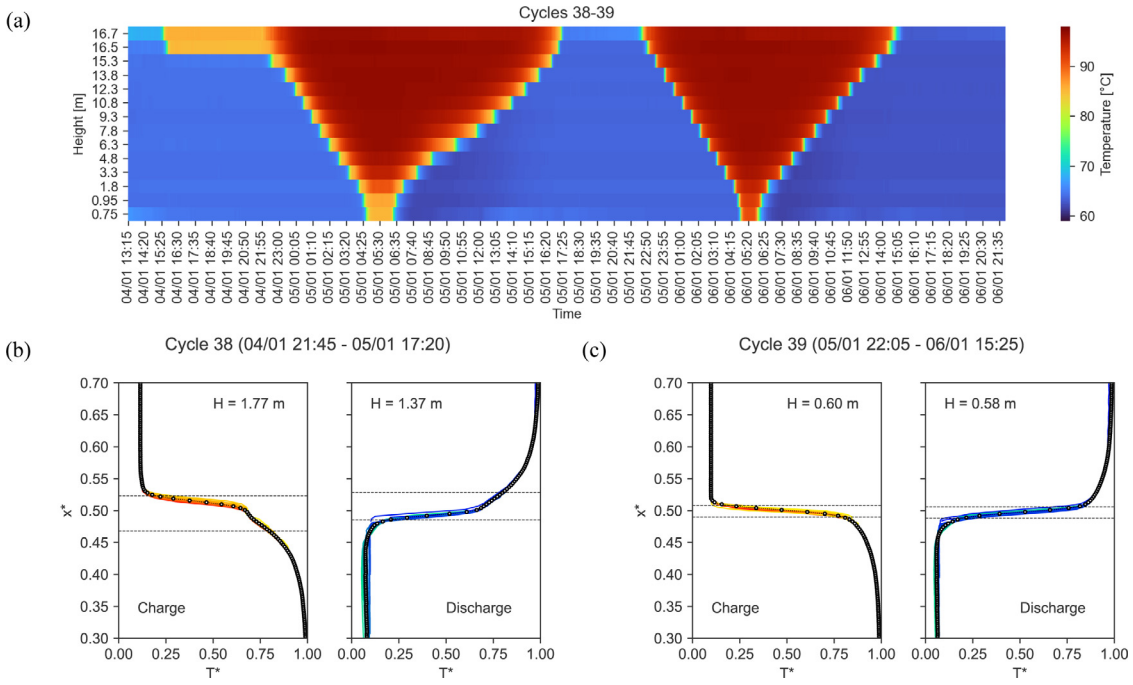


**Fig. 9.** (a) Time evolution of temperatures from the end of cycle 37 to the end of cycle 39; thermocline thickness during charge and discharge periods of cycle 38 (b) and 39 (c): bullets indicate the mean of temperature profiles from different sensors (coloured curves on the back). $x^*$ is the water mass displacement calculated as in Section 2.3, normalised over maximum value.

For all the examined cases, the momentum of energy associated with the experimental TES is close to the momentum of the perfectly stratified tank throughout the cycle, leading to stratification efficiency values often above 90% during charge and discharge periods. This order of magnitude is slightly larger than the predictions by Dahash et al. [7] for a seasonal tank of 100000 m$^3$. Fig. 10 shows an example of stratification efficiency evolution during full cycle number 50: during the discharge process, a decrease in the experimental moment of energy results in a reduction of stratification efficiency by over 10%. However, cycle 50 is the one displaying the maximum values of discharge-to-charge and exergy efficiencies (see Fig. 5). This apparent contradiction probably derives from the fact that both $\eta_{\mathrm{I}}$ and $\psi$ formulations include the time-dependent temperature of cold water returning from the users. As illustrated by the heatmap in Fig. 11, the water injected in the tank at the beginning of the discharge is colder than the one extracted during the charging process, thus increasing the temperature difference at the numerators of both $\eta_{\mathrm{I}}$ and $\psi$. This effect somehow masks the deterioration in stratification that occurs when the process slows down and stops, conversely resulting in overall high efficiency values. On the other hand, the time-dependent nature

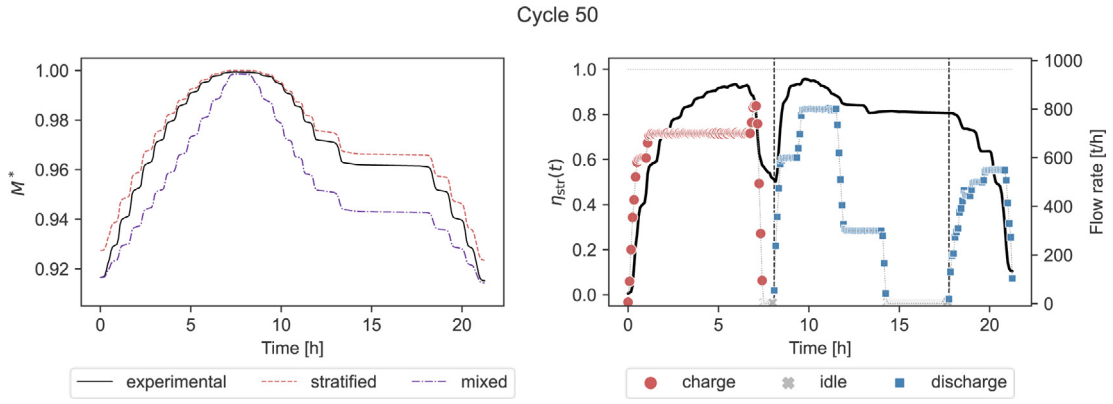


**Fig. 10.** Stratification efficiency of a full cycle (cycle ID 50). Left: moments of energy of the experimental and ideal TESs. Right: stratification efficiency (black solid line) and flow rates (markers) versus cycle time.

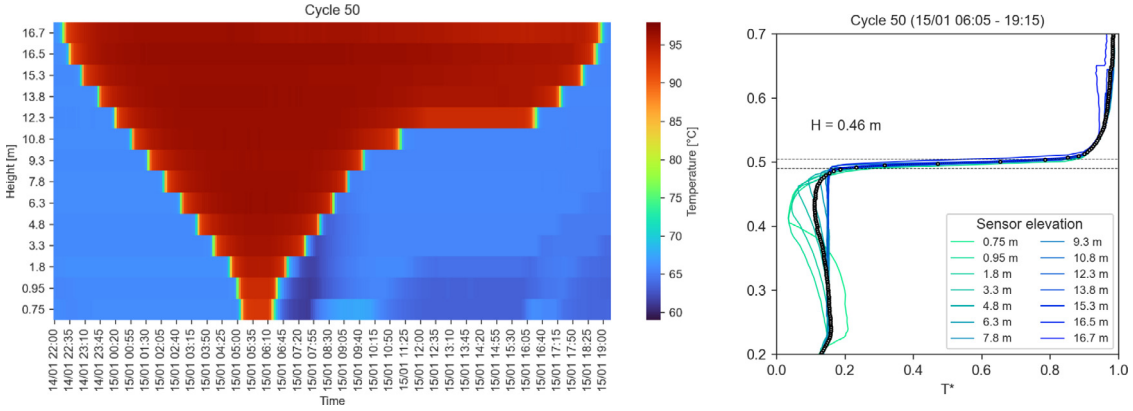


**Fig. 11.** Left: qualitative illustration of water temperature evolution in the TES during cycle 50. Right: thermocline evolution during the discharge process for the same cycle. The injection of colder water is visible both in the heatmap (lowermost layers at 6:45–7:55) and in the thermocline profiles ("noses" at low non-dimensional temperatures in the profiles from the lowermost sensors).

of $\eta_{str}(t)$ shows the evolution from the maximum at $t \approx 10$ h to the stand-by plateau. This is an example of how single-value indicators may be misleading, whereas time-dependent analyses may help in identifying significant operative aspects. As a side note, the left graph in Fig. 11 suggests that the thermocline thickness calculated on an average curve may not be an adequate measure in this specific case, as the profiles considerably change in time.

As previously mentioned, stratification number provides complementary information about the degree of mixing in the TES along time. The evolution of $Str(t)$ for the same cycle 50 analysed above is given in Fig. 12. Contrary to the trend shown in Fig. 3, the stratification number apparently decreases when the flow rate increases. However, increases in flow rates in cycle 50 happen to correspond to the injection of colder water from the bottom inlet. Recalling the definition of the stratification number, this effect causes the average gradient at the numerator to momentarily increase, resulting in higher stratification number values. Therefore, the stratification number provides an instantaneous picture of how close water temperature endpoints are in the experimental TES with respect to a reference situation.

Fig. 13 compares stratification efficiency and stratification number of cycle ID 1, characterised by low energy and exergy efficiencies (see Fig. 5): in this case, *Str* captures the reduction of the average temperature gradient due to the simultaneous effect of warmer return water at the bottom and heat transfer between the two plugs in the top portion of the TES, whereas no abrupt change can be observed in $\eta_{str}$ for the corresponding period.

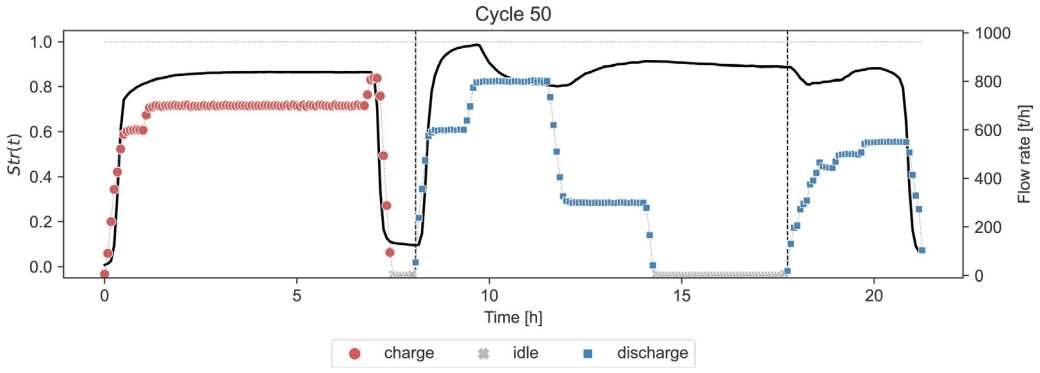


**Fig. 12.** Stratification number of cycle ID 50 (black solid line) and flow rates (markers) versus cycle time.

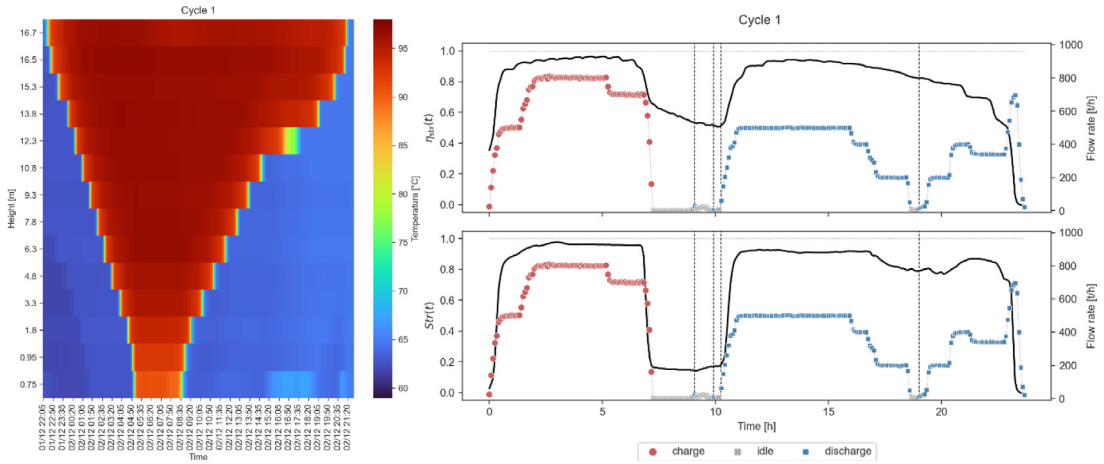


**Fig. 13.** Comparison between stratification efficiency and stratification number for cycle 1 (right). Temperature evolution during the cycle illustrated by heatmap on the right.

## 4. Summary and recommendations

The analysis of several efficiency and stratification parameters highlighted useful information both from the operative perspective and from a methodological point of view. Low flow rates and long stand-by periods seem to be detrimental to discharging performances. From the qualitative analysis of the cycles, it was found that partial charge or discharge processes followed by long stand-by/idle periods have a negative effect due to mixing/heat transfer phenomena at the interface. In particular, short charge events in a fully discharged TES (and the mirror situation of short discharge events from a fully charged TES) have the worst effect on thermocline thickness and stratification quality, as the small amount of water injected is entirely turned into a layer at an intermediate temperature that preserves until extraction. This problem is especially critical when the injected water remains upstream of the distribution device.

Estimation of thermal losses indicates that the heat transferred to the outside is a very small percentage of the heat stored, but it is higher than theoretical predictions. The reason is found in the fact that the water surface is in contact with the external environment through air vents. The installation of a membrane above the water surface could fulfil the two-fold function of a barrier against the entrainment of oxygen and the escape of evaporated fluid.

From a methodological viewpoint, the different analyses performed confirmed that the important information contained in the experimental data cannot be summarised in one indicator, but must be extracted through a combination of qualitative, single-point and time-dependent parameters. Discharge-to-charge energy efficiency and exergy both convey information about the fraction of stored energy that is made unusable during the stand-by and discharge process. Some indicators are extremely sensitive to water inlet temperatures, like charging/discharging

efficiencies, exergy efficiency and stratification number. Stratification efficiency is suitable to capture major destratification occurrences but is not very sensitive to inlet temperature fluctuations or minor variations in the temperature field. Thermocline thickness is another measure of stratification performances and can raise attention to anomalous events. The stability of the temperature profile during the cycle must be evaluated when an average thermocline thickness is used for performance evaluation. In all cases, heatmaps illustrating the time evolution of the temperature along the tank axis can be a valid support in understanding underlying phenomena.

The performances of the investigated TES are very good if compared to the figures reported in the literature for smaller and larger size tanks. In particular, stratification analysis shows that the custom-designed flow injection and distribution system successfully contributes to the limitation of the thermocline thickness and its stability in time.

## 5. Conclusions

Thermal energy storage tanks are gaining importance in the development of flexible district heating networks. The size of tanks normally installed in district heating systems is of the order of thousands of cubic metres and it is not frequently encountered in experimental studies in the literature, arguably due to difficulty in instrumenting such massive devices and extracting meaningful data. In this work, temperature and flow rate measurements continuously collected for two months in the heating season on a 5000 $m^3$ thermal energy storage of a district heating network in Brescia, Italy, have been analysed to characterise its performances under different viewpoints. Values of single-point and time-dependent indicators from the literature have been calculated, showing that the construction choices and the custom-designed inlet flow distributors confer the TES good storage and stratification performances. Particular attention must be paid to low flow rates, idle periods during discharge processes, and partial charge/discharge events followed by long stand-by intervals, all of which contribute to decreasing the stored usable energy.

Based on this evidence, it could be of help to monitor the thermocline thickness in real-time and tune the charge/discharge process so that thin thermoclines are preserved. The growing availability of experimental data acquired on different storage tanks in real operating conditions will allow to further characterise these systems and propose recommendations for their efficient operation.

## Declaration of competing interest

The authors declare that they have no known competing financial interests or personal relationships that could have appeared to influence the work reported in this paper.

## Data availability

The data that has been used is confidential.

## Acknowledgements

This study was sponsored by the Regione Lombardia project ‘Smart Grid Pilot: Banco EnergETICO’ (CUP E89I17000410009, Asse I, POR FESR 2014–2020).

## References

[1] Van Oevelen T, Scapino L, Koussa JA, Vanhoudt D. A case study on using district heating network flexibility for thermal load shifting. Energy Rep 2021;7:1–8. http://dx.doi.org/10.1016/j.egyr.2021.09.061.

[2] Guelpa E, Verda V. Thermal energy storage in district heating and cooling systems: A review. Appl Energ 2019;(252). http://dx.doi.org/10.1016/j.apenergy.2019.113474.

[3] Famiglietti J, Gerevini L, Spirito G, Pozzi M, Dénarié A, Scoccia R, Motta M. Environmental life cycle assessment scenarios for a district heating network. An Italian case study. Energy Rep 2021;7:368–79. http://dx.doi.org/10.1016/j.egyr.2021.08.094.

[4] Kallert A, Egelkamp R, Bader U, Münnich D, Staudacher L, Doderer H. A multivalent supply concept: 4th generation district heating in Moosburg an der Isar. Energy Rep 2021;7:110–8. http://dx.doi.org/10.1016/j.egyr.2021.09.032.

[5] Saloux E, Candanedo JA. Sizing and control optimization of thermal energy storage in a solar district heating system. Energy Rep 2021;7:389–400. http://dx.doi.org/10.1016/j.egyr.2021.08.092.

[6] Lou W, Luo L, Hua Y, Fan Y, Du Z. A review on the performance indicators and influencing factors for the thermocline thermal energy storage systems. Energies 2021;(14). http://dx.doi.org/10.3390/en14248384.

[7] Dahash A, Ochs F, Tosatto A. Techno-economic and exergy analysis of tank and pit thermal energy storage for renewables district heating systems. Renew Energ 2021;180:1358–79. http://dx.doi.org/10.1016/j.renene.2021.08.106.

[8] Haller MY, Cruickshank CA, Streicher W, Harrison SJ, Andersen E, Furbo S. Methods to determine stratification efficiency of thermal energy storage processes - Review and theoretical comparison. Sol Energy 2009;83:1847–60. http://dx.doi.org/10.1016/j.solener.2009.06.019.
[9] Castell A, Medrano M, Solé C, Cabeza LF. Dimensionless numbers used to characterize stratification in water tanks for discharging at low flow rates. Renew Energ 2010;35:2192–9. http://dx.doi.org/10.1016/j.renene.2010.03.020.
[10] Rendall J, Abu-Heiba A, Gluesenkamp K, Nawaz K, Worek W, Elatar A. Nondimensional convection numbers modeling thermally stratified storage tanks: Richardson's number and hot-water tanks. Renew Sust Energ Rev 2021;150. http://dx.doi.org/10.1016/j.rser.2021.111471.
[11] Piana EA, Grassi B, Socal L. A standard-based method to simulate the behavior of thermal solar systems with a stratified storage tank. Energies 2020;13(266). http://dx.doi.org/10.3390/en13010266.
[12] Fernández-Seara J, Uhía FJ, Sieres J. Experimental analysis of a domestic electric hot water storage tank. Part II: dynamic mode of operation. Appl Therm Eng 2007;27:137–44. http://dx.doi.org/10.1016/j.applthermaleng.2006.05.004.
[13] Siuta-Olcha A, Cholewa T. Experimental study of thermal stratification in a storage tank of a solar domestic hot water system. In: Pawlowski A, Dudzinska MR, Pawlowski L, editors. Environmental Engineering IV. London, UK: CRC Press LLC; 2013, p. 369–79. http://dx.doi.org/10.1201/b14894.
[14] Kumar K, Singh S. Investigating thermal stratification in a vertical hot water storage tank under multiple transient operations. Energy Rep 2021;7:7186–99. http://dx.doi.org/10.1016/j.egyr.2021.10.088.
[15] Bai Y, Wang Z, Fan J, Yang M, Li X, Chen L, Yuan G, Yang J. Numerical and experimental study of an underground water pit for seasonal heat storage. Renew Energ 2020;150:487–508. http://dx.doi.org/10.1016/j.renene.2019.12.080.
[16] Pilotelli M, Grassi B, Lezzi AM, Beretta GP. Flow models of perforated manifolds and plates for the design of a large thermal storage tank for district heating with minimal maldistribution and thermocline growth. Appl Energ 2022. http://dx.doi.org/10.1016/j.apenergy.2022.119436.
[17] A2A. A2A - New thermal energy storage at the lamarmora plant in brescia. 2020, Construction time-lapse.
[18] Zurigat YH, Ghajar AJ. Heat transfer and stratification in sensible heat storage systems. In: Thermal energy storage: systems and applications. New York: Wiley; 2002.
[19] Wang Z, Zhang H, Dou B, Huang H, Wu W, Wang Z. Experimental and numerical research of thermal stratification with a novel inlet in a dynamic hot water storage tank. Renew Energ 2017;111:353–71. http://dx.doi.org/10.1016/j.renene.2017.04.007.
[20] Davidson JH, Adams DA, Miller JA. A coefficient to characterize mixing in solar water storage tanks. J Sol Energ-T ASME 1994;116:94–9. http://dx.doi.org/10.1115/1.2930504.
[21] Andersen E, Furbo S, Fan J. Multilayer fabric stratification pipes for solar tanks. Sol Energy 2007;81:1219–26. http://dx.doi.org/10.1016/j.solener.2007.01.008.
[22] A2A. A2A - new thermal energy storages at the centrale nord plant in Brescia. 2022, Construction time-lapse.
[23] Abd Majid MA, Muhammad M, Hampo CC, Akmar AB. Analysis of a thermal energy storage tank in a large district cooling system: A case study. Processes 2020;8(1158). http://dx.doi.org/10.3390/pr8091158.